Magnetic Resonance Elastography of Human Hippocampal Subfields: CA3-Dentate Gyrus Viscoelasticity Predicts Relational Memory Accuracy

Ana M. Daugherty[1], Hillary D. Schwarb[2], Matthew D. J. McGarry[3] Curtis L. Johnson[4], and Neal J. Cohen[2]

Abstract

■ The hippocampus is necessary for binding and reconstituting information in relational memory. These essential memory functions are supported by the distinct cytoarchitecture of the hippocampal subfields. Magnetic resonance elastography is an emerging tool that provides sensitive estimates of microstructure vis-à-vis tissue mechanical properties. Here, we report the first in vivo study of human hippocampal subfield viscoelastic stiffness and damping ratio. Stiffness describes resistance of a viscoelastic tissue to a stress and is thought to reflect the relative composition of tissue at the microscale; damping ratio describes relative viscous-to-elastic behavior and is thought to generally reflect microstructural organization. Measures from the subiculum (combined with presubiculum and parasubiculum), cornu ammonis (CA) 1–2, and CA3-dentate gyrus (CA3-DG) were collected in a sample of healthy, cognitively normal men (n = 20, age = 18–33 years). In line with known cytoarchitecture, the subiculum demonstrated the lowest damping ratio, followed by CA3-DG and then combined CA1–CA2. Moreover, damping ratio of the CA3-DG—potentially reflective of number of cells and their connections—predicted relational memory accuracy and alone replicated most of the variance in performance that was explained by the whole hippocampus. Stiffness did not differentiate the hippocampal subfields and was unrelated to task performance in this sample. Viscoelasticity measured with magnetic resonance elastography appears to be sensitive to microstructural properties relevant to specific memory function, even in healthy younger adults, and is a promising tool for future studies of hippocampal structure in aging and related diseases. ■

INTRODUCTION

The hippocampus is critical to declarative or relational memory function (Eichenbaum & Cohen, 2001; Cohen & Eichenbaum, 1993), and the nature of the structure–function relation has been the focus of decades of experimental and observational study. MRI techniques have demonstrated an association of hippocampal volumetry and functional activation with memory performance across the human lifespan (Monti et al., 2015; Hannula & Ranganath, 2008; Davachi, 2006; Kirwan & Stark, 2004). These examples of neuroimaging methods, however, are gross approximations of hippocampal microstructure that is considered the neural basis of specific memory functions. Advanced imaging techniques with contrasts sensitive to tissue microstructure may provide an avenue to better understand the relation between hippocampal structure and memory function.

Magnetic resonance elastography (MRE) is a neuroimaging method that captures mechanical properties of tissue (Manduca et al., 2001; Muthupillai et al., 1995). Applying force via systematic vibration, MRE approximates the physical properties of elasticity (i.e., recovery of shape deformation after force) and viscosity (i.e., resistance to flow). Like other biological tissues, human gray and white matter have both properties and are considered mechanically viscoelastic (Budday et al., 2015). Their viscoelasticity can be described by stiffness and damping ratio properties, which serve as proxy indicators of microstructure and tissue health (Hiscox et al., 2016). Stiffness, which describes resistance of a viscoelastic tissue to a stress, is thought to reflect the relative composition of tissue at the microscale and the strength of its components (Sack, Jöhrens, Würfel, & Braun, 2013). Damping ratio, which is a dimensionless parameter that describes relative viscous-to-elastic behavior, is thought to generally reflect organization of tissue at the microscale (Sack et al., 2013). When compared between brain regions, a uniform and organized cell structure may confer greater elasticity and less viscosity, whereas less-organized tissues could appear as the opposite.

Viscoelasticity measures may offer novel insights into tissue microstructure as they reflect how components of tissue microstructure act and interact when mechanically forced, as opposed to other techniques that are related to discrete tissue elements, such as metrics from diffusion-weighted imaging. Between-person differences

[1]Wayne State University, [2]University of Illinois at Urbana-Champaign, [3]Dartmouth College, [4]University of Delaware

in regional viscoelasticity would indicate individual variability in several microstructural factors, including the number of cells and their connections. Several neurodegenerative diseases present with overall tissue softening (Murphy et al., 2016; Romano et al., 2014; Streitberger et al., 2012) that has been linked to chronic neuroinflammation (Riek et al., 2012) and demyelination (Schregel et al., 2012) in white matter regions. MRE has been most commonly applied to the study of whole brain (Streitberger et al., 2012; Murphy et al., 2011), brain lobes (Murphy et al., 2016; Arani et al., 2015), and white matter tracts (Romano et al., 2014; Johnson, McGarry, Gharibans, et al., 2013; Guo et al., 2012). The focus on large ROIs in these studies was, in part, because of methodological challenges for sufficient spatial resolution and signal accuracy in smaller regions (Johnson et al., 2014; Johnson, McGarry, Van Houten, et al., 2013).

Our research group has recently demonstrated the feasibility of applying the technique in smaller, subcortical gray matter regions, including the hippocampus (Johnson et al., 2016). Furthermore, we have evaluated the relation between hippocampal viscoelasticity (measured via adjusted damping ratio, ξ') and memory performance. Among healthy young (Schwarb, Johnson, McGarry, & Cohen, 2016) and older (Hiscox et al., 2018) adults, greater adjusted damping ratio of the hippocampus correlates with better relational memory accuracy. In an independent sample, we recently replicated the selective effect of hippocampal viscoelasticity that mediated the benefits of greater cardiorespiratory fitness on relational memory function among young adults (Schwarb et al., 2017). Furthermore, MRE estimates of viscoelasticity appear to be functionally specific by region—for example, dissociating cognitive correlates and functional activation between the hippocampus and frontal cortices (Schwarb et al., 2019; Johnson et al., 2018). These studies highlight the sensitivity and promising utility of MRE for study of the hippocampal structure–function relation in healthy and clinical populations. However, to date, MRE studies of memory correlates have focused on the total hippocampal formation that otherwise ignored the underlying complexity of the structure. The hippocampus comprises several structurally and functionally distinct subfields—the cornu ammonis (CA) fields 1–3, dentate gyrus (DG), and subiculum regions—and even greater specificity may be achieved by applying MRE to characterize the viscoelasticity of the individual regions.

The hippocampal subfields are defined by unique cytoarchitecture—cell type, size, and configuration—features that are expected to confer different viscoelastic properties. Ex vivo study of the rat hippocampus has confirmed differences in viscoelasticity between CA1, CA3, and DG subfields (Elkin, Ilankovan, & Morrison, 2011; Elkin, Azeloglu, Costa, & Morrison, 2007). A recent report on in vivo mechanical testing in the mouse hippocampus revealed differences in stiffness between hippocampal subfields that related to cell density—notably, the dentate granualar cell and CA3 pyramidal cell layers were less stiff than other subfields (Antonovaite, Beekmans, Hol, Wadman, & Iannuzzi, 2018).

The hippocampal subfields are preserved across mammalian species (Amaral & Lavenex, 2006), with few differences, and in vivo estimates of the human hippocampal viscoelastic properties from MRE are expected to similarly differentiate the subfields in line with the known cytoarchitecture. For example, the multiple layers of the presubiculum and parasubiculum are akin to the organization of the entorhinal cortex (Insausti, Muñoz-López, Insausti, & Artacho-Pérula, 2017), and the small subiculum pyramidal cells are crudely organized into columns with transverse integration (Greene & Totterdell, 1997). Thus, the subiculum regions are expected to be moderately stiff, although more elastic than viscous—that is, high adjusted damping ratio, ξ'. In contrast, the CA1 sector is expected to exhibit more viscosity—that is, low adjusted ξ'—following from the diffuse organization of pyramidal cells that are even smaller than those in CA2 and CA3 (Pyapali, Sik, Penttonen, Buzsaki, & Turner, 1998; Ishizuka, Cowan, & Amaral, 1995). The small granule cells (10-μm diameter) of the DG have an elliptical shape and are tightly packed, in most instances, without intervening glial sheath (Claiborne, Amaral, & Cowan, 1990). The U-shaped array of small cells in the DG and highly complex mossy fiber projections to the contiguous CA3 (Freund & Buzsáki, 1996; Amaral & Dent, 1981) are expected to convey an intermediate viscoelastic profile.

The past reliance on histological study has limited current understanding of the functional relevance of these microstructural features in humans, and viscoelasticity via MRE is a promising means to assess these qualities in vivo. We further aim to validate differences in viscoelasticity between hippocampal subfields by testing selective regional correlations with performance on a spatial reconstruction task that relies on relational memory function. Neurogenesis, dendrization, and pruning within the DG and CA3 are considered to underlie information binding and reconstitution in relational memory (Johnston, Shtrahman, Parylak, Gonçalves, & Gage, 2016; Rolls, 2016). Indeed, functional activation and volumes of the CA3-DG selectively correlate with relational memory performance across ages (Daugherty, Flinn, & Ofen, 2017; Yassa et al., 2011), whereas CA1 appears to be closely associated with delayed episodic recall (Bender, Daugherty, & Raz, 2013) and subiculum with general integration of information over time and space (Daugherty, Bender, Yuan, & Raz, 2016). On the basis of the known cytoarchitecture of the subfields, we hypothesized that the subiculum (combined presubiculum and parasubiculum, and subiculum) would demonstrate the greatest adjusted damping ratio, followed by combined CA3-DG, and combined CA1–CA2 (CA1-2) would have the least. Furthermore, viscoelasticity specifically in the CA3-DG, measured by greater adjusted damping ratio, would be

associated with greater relational memory accuracy. As our prior report found no correlation between hippocampal stiffness measures and performance among healthy adults (Schwarb et al., 2016), we did not expect stiffness of the subfields to predict performance as tested here.

METHODS

Participants

A sample of healthy, cognitively normal men (n = 20, age 18–33 years) participated in the study. Only men were recruited to the study because of sexual dimorphism in MRE measures—across the adult lifespan, women's brain tissue, including the temporal lobe, is more stiff than men's (Arani et al., 2015; Sack et al., 2009), although the same has not been reported of damping ratio (Schwarb et al., 2017). The sample selection improved the sensitivity of the analyses in a sample this size. We have previously reported total hippocampal MRE measures in this sample (Schwarb et al., 2016), and here, we assess novel indices in the hippocampal subfields. To be eligible for study, participants were right-handed, received at least a high school education (M = 18.70 years, SD = 3.20 years), had no history of neurological or psychiatric disease, and could undergo MRI. All participants provided informed, written consent, and the study was conducted according to procedures approved by the institutional review board.

Neuroimaging Protocol

Participants completed a 1-hr neuroimaging session in a 3-T Siemens Trio whole-body scanner with a 32-channel head receiver coil (Siemens Medical Solutions). The protocol included a high-resolution T_1-weighted MPRAGE sequence with the following parameters: 0.9-mm^3 isotropic voxel, repetition time = 1900 msec, echo time = 2.32 msec, and inversion time = 900 msec, all collected sagittally.

The MRE acquisition used a 3-D multislab, multishot spiral sequence (Johnson et al., 2014) with the following parameters: 1.6-mm^3 isotropic voxel, repetition time = 1800 msec, echo time = 73 msec, 240-mm field of view, 150 × 150 matrix size, and 60 axial slices. A pneumatic actuator (Resoundant) generated 50-Hz vibrations via a soft pillow driver placed under the participant's head. The resulting displacement fields were sampled in three directions and at four time points during a single period of vibration. Image reconstruction included correction for magnetic field inhomogeneity and motion-induced phase errors (Johnson et al., 2014). Complex, full vector displacement fields were generated in a total acquisition time of 12 min. For a comprehensive reference on the MRE technique, please see Hiscox et al. (2016).

Hippocampal Subfield Segmentation

To extract regional MRE measures, we created masks from manual segmentation of the hippocampal subfields on the high-resolution T_1-weighted MPRAGE. The masks included three regions: combined subiculum, presubiculum, and parasubiculum (Sub); CA1-2; and combined CA3 and DG (CA3-DG). The manual segmentation protocol is described in detail elsewhere (Bender et al., 2018) and is similar to one our research group has reported before (Daugherty, Bender, Ofen, & Raz, 2016). Briefly, boundaries between adjacent subfields were determined by a geometric heuristic, and visualization of the hippocampal fissure and intensity differences along it informed the internal boundary of the CA3-DG region (see Figure 1A for example segmentation). The reliability of the segmentation protocol applied to T_1-weighted MPRAGE was confirmed with mask area estimates in a sample of 10 participants after a 4-week delay with an intraclass correlation coefficient for a single rater (Shrout & Fleiss, 1979): ICC

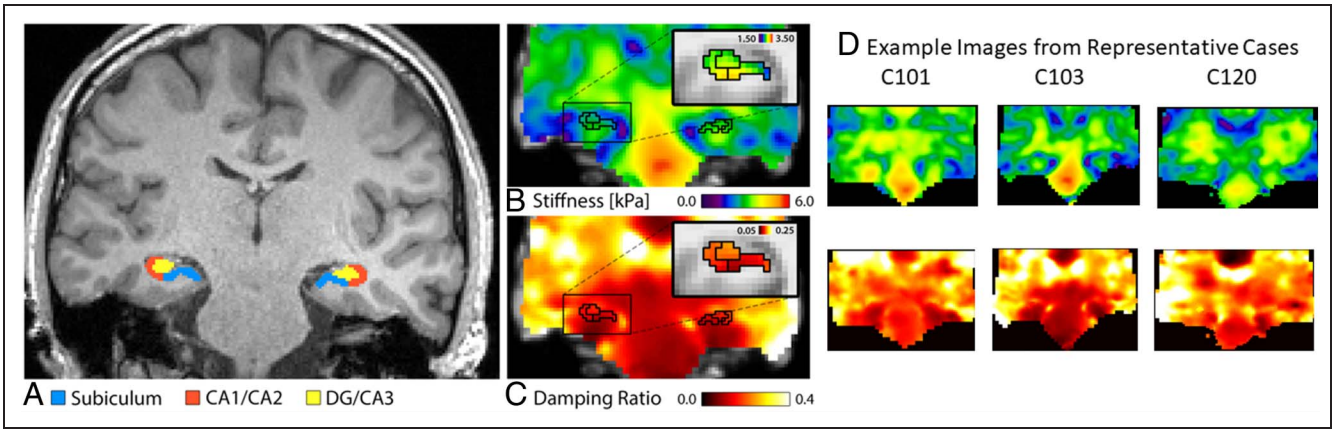

Figure 1. Example hippocampal subfield segmentation and MRE estimates. (A) Example segmentation on high-resolution T_1-weighted MPRAGE. (B–C) Average heat map of unadjusted stiffness and damping ratio estimates in the hippocampus scaled to the whole brain; insets show MRE indices scaled within the hippocampus. (D) Example MRE estimates at the level of the hippocampus, scaled to the whole brain, in three representative cases selected at random.

(3) ≥ .90 for all subfields. A similar approach has been used to create masks in functional neuroimaging studies of hippocampal subfields (e.g., Yassa et al., 2011) but is insufficient to accurately measure subfield volumetry. Thus, we limit our report to MRE measures extracted from the masks.

MRE of the Hippocampal Subfields

Mechanical tissue properties were calculated from MRE displacement images using our hippocampal elastography procedure (Johnson et al., 2016; Schwarb et al., 2016) that has been reported in detail before and is outlined here in brief. The nonlinear inversion (NLI) algorithm (McGarry et al., 2012) computed the complex-valued tissue shear modulus, $G = G' + iG''$, from MRE displacement data. We supplemented the NLI approach with subject-specific hippocampal subfield masks in MRE data space created by registering the manual segmentation masks using FLIRT in FSL (Jenkinson, Beckmann, Behrens, Woolrich, & Smith, 2012; Jenkinson, Bannister, Brady, & Smith, 2002). The masks were used as a priori spatial information in the NLI optimization routine implemented through soft prior regularization (McGarry et al., 2013), which promotes local homogeneity in each individual hippocampal subfield mask (Figure 1B and 1C). This method provides reliable measures of shear stiffness, $\mu = 2|G|^2/(|G| + G')$ (Manduca et al., 2001), and damping ratio, $\xi = G''/2G'$ (McGarry & Van Houten, 2008); specifically, coefficient of variation in repeated measurement was approximately 7% in μ estimates and 5% in ξ estimates collected in the total hippocampus (Johnson et al., 2016). Individual cases were reviewed manually for data quality after processing (see Figure 1D for example images of representative cases). Here, we report adjusted damping ratio, $\xi' = 1 - \xi$, to describe relative viscoelasticity that has demonstrated a strong correlation with relational memory, as in our previous report (Schwarb et al., 2016, 2017, 2019; Johnson et al., 2018).

Relational Memory: Spatial Reconstruction Task

We tested selective correlations of hippocampal subfield MRE with performance on a computerized spatial reconstruction task (Schwarb et al., 2016; Monti et al., 2015). The task included 20 trials, each consisting of a 20-sec study period, followed by a 4-sec delay, and then a free reconstruction period. During study, participants viewed the location of five novel, ambiguous line drawings that were randomly distributed on the screen. The stimuli then disappeared, and the screen was blank during the delay period. At reconstruction, the five objects were presented in a horizontal line at the top of the screen. Participants were instructed to then reconstruct the studied arrangement of objects on the screen, freely recalling and placing the items with the computer mouse. Reconstruction was self-paced, and participants were able to adjust their reconstruction until they were satisfied. The participants received no feedback during the task.

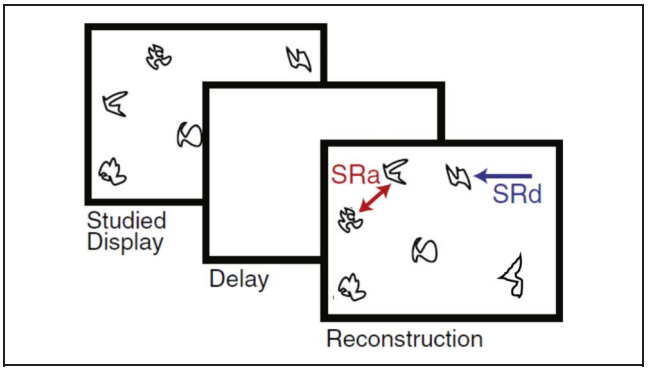

Figure 2. Schematic of the spatial reconstruction task. The task included 20 trials, each consisting of a 20-sec study period, followed by a 4-sec delay, and then a free reconstruction period. Relational memory accuracy was indexed by the total sum of average distance (SRd) and average arrangement (SRa) scores across task trials.

Relational memory accuracy was indexed by the total sum of average distance and average arrangement scores across task trials (Figure 2). Average distance and arrangement errors were then converted so that higher scores indicated better task performance. The computation of each error is described in detail in Watson, Voss, Warren, Tranel, and Cohen (2013). The distance score measure was the composite score combining misplacement errors and edge-resizing errors. Misplacement errors were computed as the distance (pixels) between an item's studied location and its placement during reconstruction, and edge-resizing errors were computed as the relative distance (i.e., vector length) between pairs of items. The arrangement score measure was the combined rearrangement errors and swap errors. Rearrangement errors refer to mistakes in configuration of the items, defined by a sign change in either the x or y dimension at any vertex. Swap errors refer to the incorrect assignment of particular items within a pair defined by a sign change on both the x and y dimensions.

Statistical Analyses

Possible differences in MRE measures of adjusted damping ratio (ξ') and stiffness (μ) between hippocampal subfields were tested in a 3 (subfield ROI) × 2 (hemisphere) repeated-measure general linear model with Huynh–Feldt corrected p values. Omnibus effects were decomposed with paired t tests including a Bonferroni correction for multiple comparisons ($\alpha' = .02$).

Confirmatory hypothesis testing with structural equation modeling was used to evaluate the hypothesized specific correlation of CA3-DG viscoelasticity with relational memory performance. This approach accounts for correlations in MRE measures between hippocampal subfields simultaneous to the hypothesis test. On the

basis of the reviewed literature (Daugherty et al., 2017; Yassa et al., 2011), the primary hypothesis tested that CA3-DG viscoelasticity predicts relational memory accuracy. A second, alternative hypothesis model tested if a nonspecific effect of MRE measures in the hippocampal body, in general, better explained differences in relational memory accuracy. The alternative hypothesis model included a latent factor reflective of all three subfields (specified loadings = 1), which is consistent with the subfields as correlated, repeated measures of the whole hippocampus and conceptually similar to a sum total estimate.

For each model, path significance ($p < .05$) and bias-corrected bootstrapped (5000 draws; Hayes & Scharkow, 2013) 95% confidence intervals (BS 95% CIs) were interpreted for the hypothesized effects. Comparing the fit between the nested models identified which hypothesis—CA3-DG as the prominent predictor or a general effect of hippocampal MRE—more reliably replicated the observed data. Comparably better fit of the hypothesized model would provide evidence of a specific effect of CA3-DG rather than a general hippocampal effect. Comparing R^2 of spatial reconstruction accuracy was considered for further evidence of CA3-DG as a single predictor that may replicate the variance explained by the whole. Nested-model fit comparisons were made with Akaike information criterion (AIC) and sample-size-adjusted Bayesian information criterion (BIC), for which relatively smaller values indicate improved model fit. The fit of the accepted model was further evaluated based on a compendium of absolute and incremental fit indices (Raykov & Marcoulides, 2006): chi-square nonsignificance, comparative fit index (> 0.90), root mean square error of approximation (≤ 0.05), and standardized root mean residual (< 0.08). The sample size limits the number of parameters estimated; thus, damping ratio and stiffness indices were tested in separate models.

RESULTS

Differences in Damping Ratio and Stiffness between Hippocampal Subfields

As expected, the mask size of the subfields differed, $F(2, 38) = 111.81$, $p < .001$, and was moderately correlated with adjusted damping ratio ξ' (right: $r = -.53$ to $-.73$, all ps $< .02$; left: $r = -.21$ to $-.27$, *ns*) and stiffness μ (right: $r = -.24$ to $-.32$, *ns*; left: $r = -.24$ to $-.28$, *ns*). Although several of the correlations were not significant in this sample, the magnitude of the effects suggests that the MRE measures are partially dependent on the size of the subfield masks. To account for this during hypothesis testing, ξ' and μ measures were corrected for hippocampal subfield mask size via regression (Jack et al., 1989), and larger values indicated greater adjusted damping ratio and stiffness, respectively. Adjusted ξ' measures were similar between hemispheres, $F(1, 19) = 0.08$, $p = .78$, whereas corrected μ measures were larger in the right hemisphere, $F(1, 19) = 13.71$, $p = .002$; in the interest of parsimony, bilateral averages were tested in further analysis.

Adjusted ξ' varied between hippocampal subfields, $F(2, 38) = 93.25$, $p < .001$: Sub demonstrated the greatest adjusted damping ratio, both ts$(19) \geq 8.21$, $p < .001$, $\alpha' = .02$, followed by CA3-DG, $t(19) = 5.14$, $p < .001$, $\alpha' = .02$, and then CA1-2 (Figure 3). Corrected μ did not significantly differ between subfields, $F(2, 38) = 3.22$, $p = .06$.

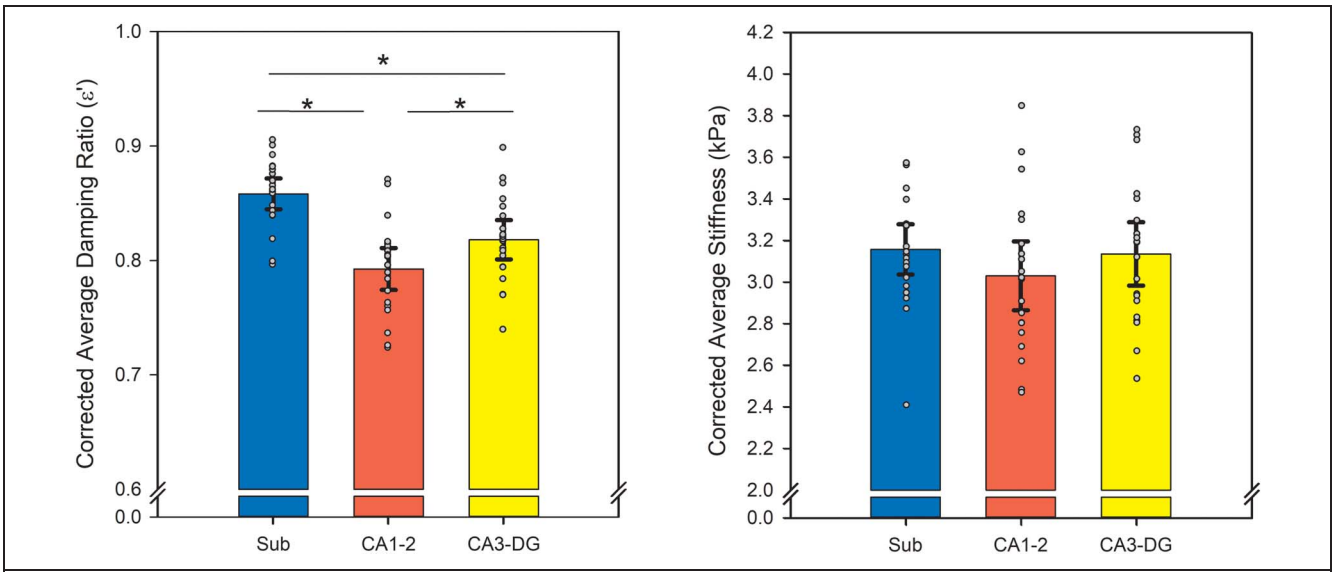

Figure 3. Differences in adjusted damping ratio (ξ') and stiffness (μ) between subfields (*$p < .05$). MRE measures were corrected for the area of the hippocampal subfield mask. Regional averages are depicted with error bars representing 2 *SEM*s, and individual observations are overlaid. Greater adjusted ξ' indicates less elasticity and more viscosity, and greater corrected μ indicates greater tissue stiffness.

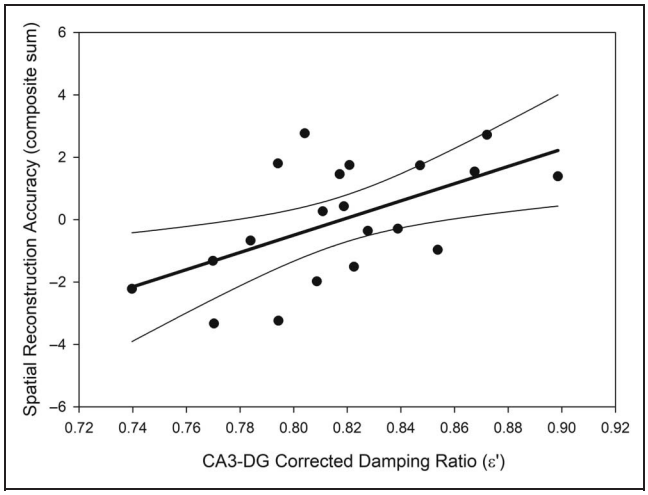

Figure 4. The association between spatial reconstruction accuracy and adjusted damping ratio in the CA3-DG. Greater viscoelasticity of the CA3-DG predicted better relational memory accuracy: b = 27.59 (standardized β = 0.56), p < .001, BS 95% CI [16.38, 39.32], and R^2 = .32. The regression line (bold) is displayed with 95% CIs.

CA3-DG Adjusted Damping Ratio Correlates with Relational Memory Accuracy

We tested the hypothesis that MRE measures within the CA3-DG, specifically, correlated with relational memory accuracy. Greater adjusted damping ratio in CA3-DG predicted greater relational memory accuracy (Figure 4): b = 27.59 (standardized β = 0.56), p < .001, BS 95% CI [16.38, 39.32]. The hypothesized model that included the CA1-2 and Sub measures as correlates of CA3-DG, but not predicting relational memory accuracy, had excellent fit and reliably reproduced the observed data: $\chi^2(2) = 0.07$, p = .97, comparative fit index = 1.00, root mean square error of approximation = 0.00, and standardized root mean residual = 0.01.

Compared to the alternative hypothesis of a general effect of hippocampal damping ratio (AIC = −177.10, BIC = −197.97), the specific effect of CA3-DG fit the data better (AIC = −181.78, BIC = −206.83). The total hippocampal damping ratio (b = 31.89, p = .003, BS 95% CI [17.51, 46.85]) accounted for 34% (R^2 = .335) of variance in spatial reconstruction accuracy, and including CA3-DG damping ratio alone replicated the effect (R^2 = .317; Figure 5). Taken together, when all subfields were included in a single model, CA3-DG damping ratio as the single predictor of relational memory accuracy reliably replicated the observed data and accounted for approximately a third of variability in performance.

Repeating the analyses with corrected μ demonstrated no significant correlation with spatial reconstruction accuracy. There was no evidence of a general effect of tissue stiffness (b = 0.26 [β = 0.04], p = .86, BS 95% CI [−1.70, 3.15]), which explained little variability in performance (R^2 = .002). There was also no evidence of a specific effect of corrected μ in CA3-DG in predicting

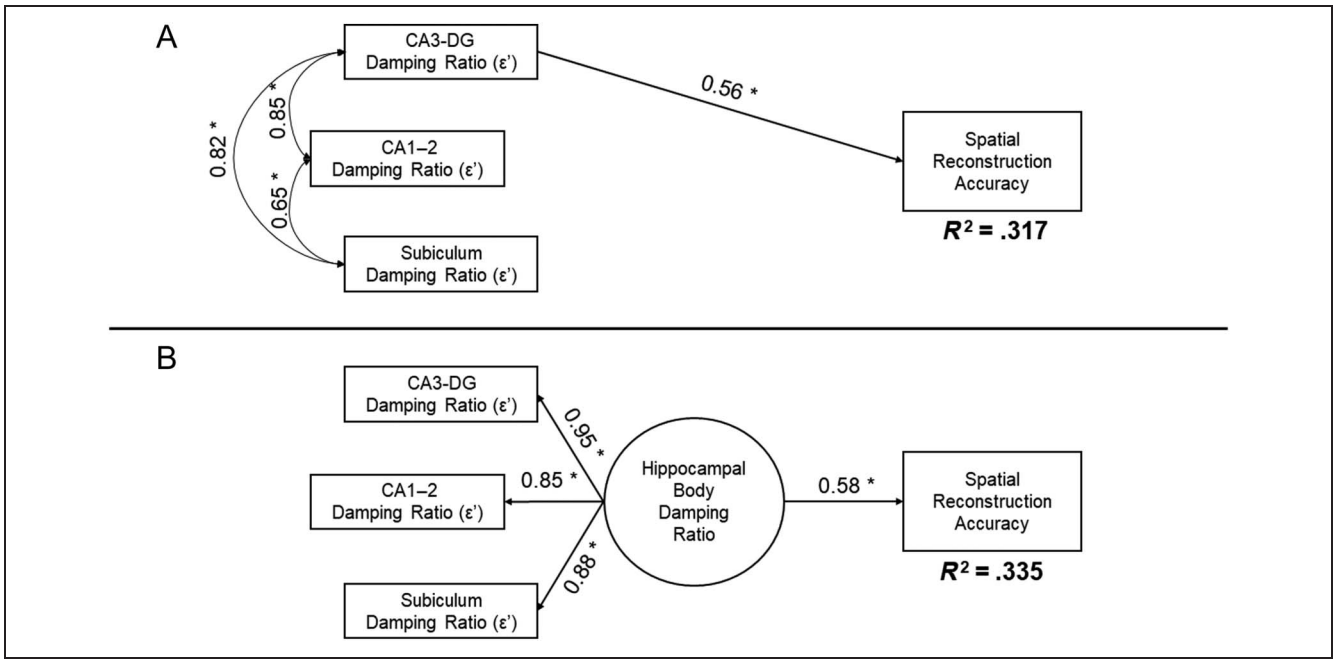

Figure 5. Comparison of primary and alternative hypothesis models testing the relation between adjusted damping ratio in hippocampal subfields and spatial reconstruction accuracy. Standardized coefficients and significance (*p < .05) are reported; R^2 estimates reflect the variance explained in spatial reconstruction accuracy by the specified model. (A) The hypothesized model tested if adjusted ε′ in the CA3-DG predicted relational memory accuracy, when including the other subfield measures as correlates that did not predict performance. (B) The alternative hypothesis model evaluates if a general effect of damping ratio within the hippocampal body accounted for variability in performance. Model fit comparisons are reported in the Results section and favored the hypothesized model. A comparison of effects illustrated here demonstrate that the measure from CA3-DG, alone, replicates the correlation observed with a general measure of hippocampal damping ratio.

performance ($b = -0.07$ [$\beta = -0.01$], $p = .95$, BS 95% CI [−1.67, 1.63]). The hypothesized (AIC = 96.10, BIC = 71.05) and alternative (AIC = 98.64, BIC = 77.77) models fit comparably. Thus, tissue stiffness did not differentiate between the hippocampal subfields and did not predict variability in relational memory accuracy in this sample of healthy, young men.

DISCUSSION

We report the first study of human hippocampal subfield viscoelasticity estimated in vivo with MRE. In healthy younger men, hippocampal subfields differed in viscoelastic damping ratio. The combined subiculum region demonstrated the greatest adjusted ξ', indicating more elastic behavior, followed by combined CA3-DG, and then combined CA1-2. This is in line with known cytoarchitecture that defines the human subfield divisions (Duvernoy, Cattin, & Risold, 2013) and ex vivo study of the rat hippocampus (Elkin et al., 2007, 2011). Moreover, greater adjusted damping ratio—potentially reflective of the number of cells and their connections—specifically in the CA3-DG predicted greater relational memory accuracy, explaining approximately 32% of individual differences in performance.

The differences in viscoelasticity between hippocampal subfields plausibly stem from the regional cytoarchitecture. The combined Sub region includes the layered organization of the presubiculum and parasubiculum and the crude columns of the subiculum (Insausti et al., 2017; Greene & Totterdell, 1997), which is potentially reflected in the Sub having the greatest adjusted ξ' (more elastic behavior) among the subfields. In contrast, the CA1 has small pyramidal cells, and its 14 million neurons (West, Coleman, Flood, & Troncoso, 1994) are relatively evenly spaced throughout the volume (Pyapali et al., 1998), which could confer more viscous behavior (lower adjusted ξ') because of energy dissipation from microstructural interactions when force is applied (Sack et al., 2013). Finally, the intermediate adjusted ξ' of CA3-DG parallels the tightly packed elliptical dentate cells (Claiborne et al., 1990) and complex mossy fiber projections to CA3 pyramidal cells (Freund & Buzsáki, 1996; Amaral & Dent, 1981). The tight organization of these interlocked regions is underscored by the sheer number of cells observed within the small volumes: Estimates in human hippocampi are as great as 18 million neurons in the dentate granule cell layer and 2.83 million in the CA3 (West et al., 1994). Thus, the pattern of differences in MRE viscoelasticity between the subfields observed here in vivo appear to agree with the known cytoarchitecture that defines the regions. Indeed, the relative difference between CA1-2 and CA3-DG damping ratio reported here is similar to viscous properties reported in an ex vivo study of the rat hippocampus (Elkin et al., 2007, 2011).

The cell types and configurations that are unique to each hippocampal subfield underlie the specificity of function of each region. For example, the CA3-DG regions serve pattern separation and completion computations, which are necessary for binding and reconstituting information in relational memory (Rolls, 2016; Yassa & Stark, 2011). Neurogenesis, dendrization, and synaptic pruning within these regions are the putative neural basis of relational memory function (Johnston et al., 2016; Rolls, 2016). Here, individuals who had CA3-DG regions with higher adjusted ξ' displayed greater relational memory accuracy. Thus, higher adjusted ξ' may reflect a richer cellular network in the CA3-DG, and those individuals may have been better equipped to encode and recall the new relational memory information presented in the task. This is consistent with other neuroimaging studies, in which larger CA3-DG volumes (Dillon et al., 2017; Shing et al., 2011) and regional functional activation (Azab, Stark, & Stark, 2014; Yassa et al., 2011) in adults correlated with performance on relational memory tasks. This is also in line with our previous reports of greater ξ' in the whole hippocampus positively correlating with relational memory performance (Johnson et al., 2018; Schwarb et al., 2016, 2017). Future longitudinal study over short time windows will be necessary to determine the sensitivity of MRE to the dynamic microstructural changes within the hippocampus in the course of memory formation and recall. Yet, the evidence of a specific association between CA3-DG adjusted damping ratio and relational memory accuracy lends credence to the notion that MRE is a sensitive approximation of the relevant microstructure. Moreover, adjusted ξ' of CA3-DG alone explained approximately 32% of individual differences in relational memory among healthy, younger adults—a segment of the population that commonly displays little variability in volumetry.

MRE appears to be more sensitive to differences in tissue microstructure than volume alone (Schwarb et al., 2016). Variability in brain region damping ratio has been linked to inflammation (Riek et al., 2012) and cardiorespiratory fitness (Schwarb et al., 2017)—modifiable health factors to which the hippocampus is superbly sensitive (Michaelis, 2012). In the rat, age-related differences in hippocampal damping ratio suggest lesser structural integrity in older brains and age effects are differential across subfields (Elkin et al., 2011; Elkin, 2009).

Volumetric study of the human brain has revealed similar age-related differences in hippocampal subfields (Daugherty, Bender, Ofen, et al., 2016) and differential vulnerability of the subfields to expressed and genetic risk of inflammation and poor vascular function (Raz, Daugherty, Bender, Dahle, & Land, 2015; Kerchner et al., 2014; Bender et al., 2013; Shing et al., 2011; Mueller & Weiner, 2009). The complementary study of MRE and volumetry in aging and cardiovascular disease would be a natural extension of the present report. Among healthy younger adults, adjusted damping ratio,

but not stiffness, differentiated the subfields and accounted for individual differences in relational memory. Tissue stiffness appears to be a marker of pathology, as demonstrated in several studies of aging and neurodegenerative diseases, including Alzheimer's disease (Murphy et al., 2016; Arani et al., 2015; Romano et al., 2014; Streitberger et al., 2012; Sack, Streitberger, Krefting, Paul, & Braun, 2011). Because of the interest in early detection of changes in hippocampal microstructure in the course of Alzheimer's disease and related dementia, the application of MRE is a promising direction for future research.

Several limitations should be considered of the present report. First, the resolution and contrast of the structural MRI analyzed here were insufficient to visualize unique cell features that are commonly used in histological study to define the boundaries between hippocampal subfields (Wisse et al., 2017). The MRI from which subfield masks were created could not accommodate accurate measurement of subfield volumes, which may account for additional variability in relational memory performance; we cannot presently evaluate this hypothesis. Although our current MRE protocol differentiates the hippocampal subfields and enjoys some construct validity based on known cytoarchitecture and regional function, the resolution of the MRE sequence may not be optimal for accurately resolving the damping ratio of the small structures given the dependence of quantitative MRE measures on spatial resolution (Johnson et al., 2014; Johnson, McGarry, Van Houten, et al., 2013). Future studies should employ high-resolution T_2-weighted imaging for subfield volumetry in conjunction with high-resolution MRE methods to further improve specificity of subfield measurements. The evidence we provide here in a sample of healthy, young adults underscores the promise of this approach, and further investing in MRE as a research tool is propitious. In addition, the sample size necessitated testing hypotheses by multiple models. The evident effect sizes and bias-corrected BS 95% CIs support the conclusion that MRE measures are sensitive correlates of individual differences in memory. Nonetheless, the smaller sample of young men and the use of a single relational memory task limit the generalizability of the reported analyses. Finally, the cross-sectional study design prohibits tests of causality, and future longitudinal study is necessary to further understand the direct link between in vivo MRE and relational memory function.

Conclusions

We report the first in vivo MRE evidence of differences in viscoelasticity between human hippocampal subfields. In a sample of healthy, young men, the Sub demonstrated the greatest adjusted damping ratio (most elastic behavior), followed by combined CA3-DG, and then combined CA1-2 (most viscous behavior). Furthermore, greater adjusted damping ratio of CA3-DG correlated with greater relational memory accuracy. MRE offers a sensitive estimate of hippocampal microstructure that underlies complex memory functions and is a promising approach to future studies of neurodegeneration in aging and related diseases.

Acknowledgments

This study was partially supported by National Institutes of Health (NIH)/National Institute of Mental Health Grant R01-MH062500, NIH/National Institute of Aging Grant R01-AG058853, and NIH/National Institute of Biomedical Imaging and Bioengineering Grants R01-EB027577 and R01-EB001981. This work was carried out in part at the Biomedical Imaging Center of the Beckman Institute for Advanced Science and Technology at the University of Illinois. We thank the Blue Waters sustained-petascale computing project at the National Center for Supercomputing Applications at the University of Illinois who provided computational resources as in the last article. Ana M. Daugherty was supported by a Beckman Institute Postdoctoral Fellowship at the University of Illinois at Urbana-Champaign, with funding provided by the Arnold and Mabel Beckman Foundation.

Reprint requests should be sent to Ana M, Daugherty, 5057 Woodward Ave., 7th fl., Psychology Department, Wayne State University, Detroit, MI 48201, or via e-mail: ana.daugherty@wayne.edu.

REFERENCES

Amaral, D. G., & Dent, J. A. (1981). Development of the mossy fibers of the dentate gyrus: I. A light and electron microscopic study of the mossy fibers and their expansions. *Journal of Comparative Neurology*, *195*, 51–86.

Amaral, D. G., & Lavenex, P. (2006). Hippocampal neuroanatomy. In P. Andersen, R. Morris, D. Amaral, T. Bliss, & J. O'Keefe (Eds.), *The hippocampus book. Oxford Neuroscience Series* (pp. 37–107). Oxford: Oxford University Press.

Antonovaite, N., Beekmans, S. V., Hol, E. M., Wadman, W. J., & Iannuzzi, D. (2018). Regional variations in stiffness in live mouse brain tissue determined by depth-controlled indentation mapping. *Scientific Reports*, *8*, 12517.

Arani, A., Murphy, M. C., Glaser, K. J., Manduca, A., Lake, D. S., Kruse, S. A., et al. (2015). Measuring the effects of aging and sex on regional brain stiffness with MR elastography in healthy older adults. *Neuroimage*, *111*, 59–64.

Azab, M., Stark, S. M., & Stark, C. E. L. (2014). Contributions of human hippocampal subfields to spatial and temporal pattern separation. *Hippocampus*, *24*, 293–302.

Bender, A. R., Daugherty, A. M., & Raz, N. (2013). Vascular risk moderates associations between hippocampal subfield volumes and memory. *Journal of Cognitive Neuroscience*, *25*, 1851–1862.

Bender, A. R., Keresztes, A., Bodammer, N. C., Shing, Y. L., Werkle-Bergner, M., Daugherty, A. M., et al. (2018). Optimization and validation of automated hippocampal subfield segmentation across the lifespan. *Human Brain Mapping*, *39*, 916–931.

Budday, S., Nay, R., de Rooij, R., Steinmann, P., Wyrobek, T., Ovaert, T. C., et al. (2015). Mechanical properties of gray and white matter brain tissue by indentation. *Journal of the Mechanical Behavior of Biomedical Materials*, *46*, 318–330.

Claiborne, B. J., Amaral, D. G., & Cowan, W. M. (1990). Quantitative, three-dimensional analysis of granule cell dendrites in the rat dentate gyrus. *Journal of Comparative Neurology*, *302*, 206–219.

Cohen, N. J., & Eichenbaum, H. (1993). *Memory, amnesia, and the hippocampal system*. Cambridge, MA: MIT Press.
Daugherty, A. M., Bender, A. R., Ofen, N., & Raz, N. (2016). Age differences in hippocampal subfield volumes from childhood to late adulthood. *Hippocampus*, *26*, 220–228.
Daugherty, A. M., Bender, A. R., Yuan, P., & Raz, N. (2016). Changes in search path complexity and length during learning of a virtual water maze: Age differences and differential associations with hippocampal subfield volumes. *Cerebral Cortex*, *26*, 2391–2401.
Daugherty, A. M., Flinn, R., & Ofen, N. (2017). Hippocampal CA3-dentate gyrus volume uniquely linked to improvement in associative memory from childhood to adulthood. *Neuroimage*, *153*, 75–85.
Davachi, L. (2006). Item, context and relational episodic encoding in humans. *Current Opinion in Neurobiology*, *16*, 693–700.
Dillon, S. E., Tsivos, D., Knight, M., McCann, B., Pennington, C., Shiel, A. I., et al. (2017). The impact of ageing reveals distinct roles for human dentate gyrus and CA3 in pattern separation and object recognition memory. *Scientific Reports*, *7*, 14069.
Duvernoy, H. M., Cattin, F., & Risold, P.-Y. (2013). *The human hippocampus: Functional anatomy, vascularization and serial sections with MRI* (4th ed.). New York: Springer-Verlag.
Eichenbaum, H., & Cohen, N. J. (2001). *From conditioning to conscious recollection: Memory systems of the brain*. Oxford: Oxford University Press.
Elkin, B. S. (2009). Age-dependent regional mechanical properties of the rat hippocampus and cortex. *Journal of Biomechanical Engineering*, *132*, 011010.
Elkin, B. S., Azeloglu, E. U., Costa, K. D., & Morrison, B., III. (2007). Mechanical heterogeneity of the rat hippocampus measured by atomic force microscope indentation. *Journal of Neurotrauma*, *24*, 812–822.
Elkin, B. S., Ilankovan, A. I., & Morrison, B. (2011). A detailed viscoelastic characterization of the P17 and adult rat brain. *Journal of Neurotrauma*, *28*, 2235–2244.
Freund, T. F., & Buzsáki, G. (1996). Interneurons of the hippocampus. *Hippocampus*, *6*, 347–470.
Greene, J. R. T., & Totterdell, S. (1997). Morphology and distribution of electrophysiologically defined classes of pyramidal and nonpyramidal neurons in rat ventral subiculum in vitro. *Journal of Comparative Neurology*, *380*, 395–408.
Guo, J., Posnansky, O., Hirsch, S., Scheel, M., Taupitz, M., Braun, J., et al. (2012). Fractal network dimension and viscoelastic powerlaw behavior: II. An experimental study of structure-mimicking phantoms by magnetic resonance elastography. *Physics in Medicine and Biology*, *57*, 4041–4053.
Hannula, D. E., & Ranganath, C. (2008). Medial temporal lobe activity predicts successful relational memory binding. *Journal of Neuroscience*, *28*, 116–124.
Hayes, A. F., & Scharkow, M. (2013). The relative trustworthiness of inferential tests of the indirect effect in statistical mediation analysis: Does method really matter? *Psychological Science*, *24*, 1918–1927.
Hiscox, L. V., Johnson, C. L., Barnhill, E., McGarry, M. D., Huston, J., van Beek, E. J., et al. (2016). Magnetic resonance elastography (MRE) of the human brain: Technique, findings and clinical applications. *Physics in Medicine and Biology*, *61*, R401–R437.
Hiscox, L. V., Johnson, C. L., McGarry, M. D., Schwarb, H., van Beek, E. J., Roberts, N., et al. (2018). Hippocampal viscoelasticity and episodic memory performance in healthy older adults examined with magnetic resonance elastography. *Brain Imaging and Behavior*, *14*, 175–185.
Insausti, R., Muñoz-López, M., Insausti, A. M., & Artacho-Pérula, E. (2017). The human periallocortex: Layer pattern in presubiculum, parasubiculum and entorhinal cortex. A review. *Frontiers in Neuroanatomy*, *11*, 84.
Ishizuka, N., Cowan, W. M., & Amaral, D. G. (1995). A quantitative analysis of the dendritic organization of pyramidal cells in the rat hippocampus. *Journal of Comparative Neurology*, *362*, 17–45.
Jack, C. R., Twomey, C., Zinsmeister, A. R., Sharbrough, F. W., Petersen, R. C., & Cascino, G. D. (1989). Anterior temporal lobes and hippocampal formations: Normaive volumetric measurements from MR Images in young adults. *Radiology*, *172*, 549–554.
Jenkinson, M., Bannister, P., Brady, M., & Smith, S. (2002). Improved optimization for the robust and accurate linear registration and motion correction of brain images. *Neuroimage*, *17*, 825–841.
Jenkinson, M., Beckmann, C. F., Behrens, T. E., Woolrich, M. W., & Smith, S. M. (2012). FSL. *Neuroimage*, *62*, 782–790.
Johnson, C. L., Holtrop, J. L., McGarry, M. D., Weaver, J. B., Paulsen, K. D., Georgiadis, J. G., et al. (2014). 3D multislab, multishot acquisition for fast, whole-brain MR elastography with high signal-to-noise efficiency. *Magnetic Resonance in Medicine*, *71*, 477–485.
Johnson, C. L., McGarry, M. D., Gharibans, A. A., Weaver, J. B., Paulsen, K. D., Wang, H., et al. (2013). Local mechanical properties of white matter structures in the human brain. *Neuroimage*, *79*, 145–152.
Johnson, C. L., McGarry, M. D., Van Houten, E. E., Weaver, J. B., Paulsen, K. D., Sutton, B. P., et al. (2013). Magnetic resonance elastography of the brain using multishot spiral readouts with self-navigated motion correction. *Magnetic Resonance in Medicine*, *70*, 404–412.
Johnson, C. L., Schwarb, H., Horecka, K. M., McGarry, M. D., Hillman, C. H., Kramer, A. F., et al. (2018). Double dissociation of structure-function relationships in memory and fluid intelligence observed with magnetic resonance elastography. *Neuroimage*, *171*, 99–106.
Johnson, C. L., Schwarb, H., McGarry, M. D., Anderson, A. T., Huesmann, G. R., Sutton, B. P., et al. (2016). Viscoelasticity of subcortical gray matter structures. *Human Brain Mapping*, *37*, 4221–4233.
Johnston, S. T., Shtrahman, M., Parylak, S., Gonçalves, J. T., & Gage, F. H. (2016). Paradox of pattern separation and adult neurogenesis: A dual role for new neurons balancing memory resolution and robustness. *Neurobiology of Learning and Memory*, *129*, 60–68.
Kerchner, G. A., Berdnik, D., Shen, J. C., Bernstein, J. D., Fenesy, M. C., Deutsch, G. K., et al. (2014). APOE ε4 worsens hippocampal CA1 apical neuropil atrophy and episodic memory. *Neurology*, *82*, 691–697.
Kirwan, C. B., & Stark, C. E. (2004). Medial temporal lobe activation during encoding and retrieval of novel face-name pairs. *Hippocampus*, *14*, 919–930.
Manduca, A., Oliphant, T. E., Dresner, M. A., Mahowald, J. L., Kruse, S. A., Amromin, E., et al. (2001). Magnetic resonance elastography: Non-invasive mapping of tissue elasticity. *Medical Image Analysis*, *5*, 237–254.
McGarry, M. D., Johnson, C. L., Sutton, B. P., Van Houten, E. E., Georgiadis, J. G., Weaver, J. B., et al. (2013). Including spatial information in nonlinear inversion MR elastography using soft prior regularization. *IEEE Transactions on Medical Imaging*, *32*, 1901–1909.
McGarry, M. D., & Van Houten, E. E. (2008). Use of a Rayleigh damping model in elastography. *Medical & Biological Engineering & Computing*, *46*, 759–766.
McGarry, M. D., Van Houten, E. E., Johnson, C. L., Georgiadis, J. G., Sutton, B. P., Weaver, J. B., et al. (2012). Multiresolution

MR elastography using nonlinear inversion. *Medical Physics*, *39*, 6388–6396.
Michaelis, E. K. (2012). *Selective neuronal vulnerability in the hippocampus: Relationship to neurological diseases and mechanisms for differential sensitivity of neurons to stress*. Oxford: Oxford University Press.
Monti, J. M., Cooke, G. E., Watson, P. D., Voss, M. W., Kramer, A. F., & Cohen, N. J. (2015). Relating hippocampus to relational memory processing across domains and delays. *Journal of Cognitive Neuroscience*, *27*, 234–245.
Mueller, S. G., & Weiner, M. W. (2009). Selective effect of age, Apo e4, and Alzheimer's disease on hippocampal subfields. *Hippocampus*, *19*, 558–564.
Murphy, M. C., Huston, J., Jack, C. R., Glaser, K. J., Manduca, A., Felmlee, J. P., et al. (2011). Decreased brain stiffness in Alzheimer's disease determined by magnetic resonance elastography. *Journal of Magnetic Resonance Imaging*, *34*, 494–498.
Murphy, M. C., Jones, D. T., Jack, C. R., Glaser, K. J., Senjem, M. L., Manduca, A., et al. (2016). Regional brain stiffness changes across the Alzheimer's disease spectrum. *Neuroimage: Clinical*, *10*, 283–290.
Muthupillai, R., Lomas, D. J., Rossman, P. J., Greenleaf, J. F., Manduca, A., & Ehman, R. L. (1995). Magnetic resonance elastography by direct visualization of propagating acoustic strain waves. *Science*, *269*, 1854–1857.
Pyapali, G. K., Sik, A., Penttonen, M., Buzsaki, G., & Turner, D. A. (1998). Dendritic properties of hippocampal CA1 pyramidal neurons in the rat: Intracellular staining in vivo and in vitro. *Journal of Comparative Neurology*, *391*, 335–352.
Raykov, T., & Marcoulides, G. A. (2006). *A first course in structural equation modeling* (2nd ed.). Mahwah, NJ: Erlbaum.
Raz, N., Daugherty, A. M., Bender, A. R., Dahle, C. L., & Land, S. (2015). Volume of the hippocampal subfields in healthy adults: Differential associations with age and a pro-inflammatory genetic variant. *Brain Structure and Function*, *220*, 2663–2674.
Riek, K., Millward, J. M., Hamann, I., Mueller, S., Pfueller, C. F., Paul, F., et al. (2012). Magnetic resonance elastography reveals altered brain viscoelasticity in experimental autoimmune encephalomyelitis. *Neuroimage: Clinical*, *1*, 81–90.
Rolls, E. T. (2016). Pattern separation, completion, and categorisation in the hippocampus and neocortex. *Neurobiology of Learning and Memory*, *129*, 4–28.
Romano, A., Guo, J., Prokscha, T., Meyer, T., Hirsch, S., Braun, J., et al. (2014). In vivo waveguide elastography: Effects of neurodegeneration in patients with amyotrophic lateral sclerosis. *Magnetic Resonance in Medicine*, *72*, 1755–1761.
Sack, I., Beierbach, B., Wuerfel, J., Klatt, D., Hamhaber, U., Papazoglou, S., et al. (2009). The impact of aging and gender on brain viscoelasticity. *Neuroimage*, *46*, 652–657.
Sack, I., Jöhrens, K., Würfel, J., & Braun, J. (2013). Structure-sensitive elastography: On the viscoelastic powerlaw behavior of in vivo human tissue in health and disease. *Soft Matter*, *9*, 5672.
Sack, I., Streitberger, K.-J., Krefting, D., Paul, F., & Braun, J. (2011). The influence of physiological aging and atrophy on brain viscoelastic properties in humans. *PLoS One*, *6*, e23451.
Schregel, K., Wuerfel, E., Garteiser, P., Gemeinhardt, I., Prozorovski, T., Aktas, O., et al. (2012). Demyelination reduces brain parenchymal stiffness quantified in vivo by magnetic resonance elastography. *Proceedings of the National Academy of Sciences, U.S.A.*, *109*, 6650–6655.
Schwarb, H., Johnson, C. L., Daugherty, A. M., Hillman, C. H., Kramer, A. F., Cohen, N. J., et al. (2017). Aerobic fitness, hippocampal viscoelasticity, and relational memory performance. *Neuroimage*, *153*, 179–188.
Schwarb, H., Johnson, C. L., Dulas, M. R., McGarry, M. D. J., Holtrop, J. L., Watson, P. D., et al. (2019). Structural and functional MRI evidence for distinct medial temporal and prefrontal roles in context-dependent relational memory. *Journal of Cognitive Neuroscience*, *31*, 1857–1872.
Schwarb, H., Johnson, C. L., McGarry, M. D., & Cohen, N. J. (2016). Medial temporal lobe viscoelasticity and relational memory performance. *Neuroimage*, *132*, 534–541.
Shing, Y. L., Rodrigue, K. M., Kennedy, K. M., Fandakova, Y., Bodammer, N., Werkle-Bergner, M., et al. (2011). Hippocampal subfield volumes: Age, vascular risk, and correlation with associative memory. *Frontiers in Aging Neuroscience*, *3*, 2.
Shrout, P. E., & Fleiss, J. L. (1979). Intraclass correlations: Uses in assessing rater reliability. *Psychological Bulletin*, *86*, 420–428.
Streitberger, K.-J., Sack, I., Krefting, D., Pfüller, C., Braun, J., Paul, F., et al. (2012). Brain viscoelasticity alteration in chronic-progressive multiple sclerosis. *PLoS One*, *7*, e29888.
Watson, P. D., Voss, J. L., Warren, D. E., Tranel, D., & Cohen, N. J. (2013). Spatial reconstruction by patients with hippocampal damage is dominated by relational memory errors. *Hippocampus*, *23*, 570–580.
West, M. J., Coleman, P. D., Flood, D. G., & Troncoso, J. C. (1994). Differences in the pattern of hippocampal neuronal loss in normal ageing and Alzheimer's disease. *Lancet*, *344*, 769–772.
Wisse, L. E. M., Daugherty, A. M., Olsen, R. K., Berron, D., Carr, V. A., Stark, C. E. L., et al. (2017). A harmonized segmentation protocol for hippocampal and parahippocampal subregions: Why do we need one and what are the key goals?: A harmonized hippocampal subfield protocoL: Key goals and impact. *Hippocampus*, *27*, 3–11.
Yassa, M. A., Lacy, J. W., Stark, S. M., Albert, M. S., Gallagher, M., & Stark, C. E. L. (2011). Pattern separation deficits associated with increased hippocampal CA3 and dentate gyrus activity in nondemented older adults. *Hippocampus*, *21*, 968–979.
Yassa, M. A., & Stark, C. E. L. (2011). Pattern separation in the hippocampus. *Trends in Neurosciences*, *34*, 515–525.